Colloids and Surfaces A: Physicochem. Eng. Aspects 464 (2015) 46–51

Contents lists available at ScienceDirect

Colloids and Surfaces A: Physicochemical and Engineering Aspects

journal homepage: www.elsevier.com/locate/colsurfa

Polymer-assisted size control of water-dispersible iron oxide nanoparticles in range between 15 and 100 nm

Pablo Tancredi[a,b], Santiago Botasini[b], Oscar Moscoso-Londoño[a], Eduardo Méndez[b], Leandro Socolovsky[a,*]

[a] Laboratorio de Sólidos Amorfos (LSA), INTECIN, Facultad de Ingeniería, Universidad de Buenos Aires – CONICET, C1063ACV Buenos Aires, Argentina
[b] Laboratorio de Biomateriales, Instituto de Química Biológica, Facultad de Ciencias, Universidad de la República, 11400 Montevideo, Uruguay

HIGHLIGHTS

- Coated Fe_3O_4 nanoparticles were synthesized by the precipitation oxidation method.
- Starch can be employed as an effective control agent to tune the nanoparticle size.
- Starch coated nanoparticles are water dispersible and forms a ferrofluid.
- Nature of the employed polymer defines the efficiency of the size-control process.

GRAPHICAL ABSTRACT

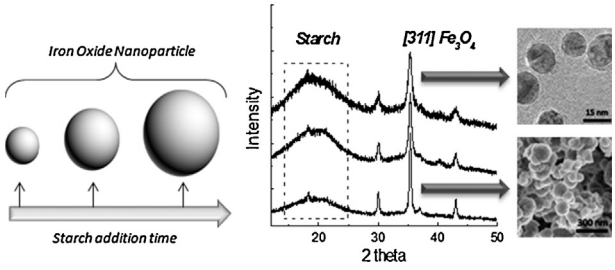

ARTICLE INFO

Article history:
Received 21 July 2014
Received in revised form
29 September 2014
Accepted 2 October 2014
Available online 12 October 2014

Keywords:
Iron oxide nanoparticles
Starch
Nanoparticles size-control
Ferrofluid
Superparamagnetism

ABSTRACT

Starch-coated Fe_3O_4 nanoparticles were synthesized by the precipitation–oxidation of ferrous hydroxide method. Starch was employed as a kinetic control agent, and the effect of the polymer on both size and aggregation of the Fe_3O_4 nanoparticles was studied. The size of the as-prepared magnetite nanoparticles was tuned from 15 to 100 nm by changing the time of addition of a starch solution on the reaction system. Also, the starch-coating over Fe_3O_4 nanoparticles assures good water-dispersibility, stability, and possible biocompatibility. Transmission and scanning electron microscopies (TEM, SEM), X-ray diffraction (XRD), Fourier Transform Infrared Spectroscopy (FTIR) and magnetic measurements were used to characterize the prepared samples.

Kinetic control assays were also done with polyethylene glycol and polyvinyl alcohol in order to study the influence of the polymer nature in the size and aggregation process of the Fe_3O_4 nanoparticles. For this work, the effect is more pronounced for voluminous polymers, with large electrosteric hindrance produced by increased polar groups per monomer, like starch.

1. Introduction

Magnetic iron oxide nanoparticles (IONPs) systems (mainly magnetite, Fe_3O_4, and maghemite, γ-Fe_2O_3) have been synthetized and studied for several years, but recently they have gained special consideration and attraction due to their technological applications associated to their nanosize-related magnetic properties [1]. These technological applications include recording media devices, chemical sensors [2], magnetic ferrofluids employed in seals, dampers or loudspeakers, as well as many biomedical uses such as biomolecule

* Corresponding author at: C1063ACV Av. Paseo Colón 850, Buenos Aires, Argentina. Tel.: +54 11 4342 1396.
E-mail addresses: ptancredi@fi.uba.ar (P. Tancredi), sbotasini@fcien.edu.uy (S. Botasini), omoscoso@fi.uba.ar (O. Moscoso-Londoño), emendez@fcien.edu.uy (E. Méndez), lsocolovsky@fi.uba.ar (L. Socolovsky).

http://dx.doi.org/10.1016/j.colsurfa.2014.10.001
0927-7757/

separation, drug targeting, magnetic hyperthermia, and contrast agents for nuclear magnetic resonance images [3,4].

Novel and diverse routes to synthesize IONPs have been reported in the last years, like thermal decomposition of organometallic precursors [5], polyol process [6,7] or reverse micelles [8]. However, the classical procedures in aqueous media remain as the most popular methods because of their operational and economic viability. Co-precipitation of Fe(II)/Fe(III) ions is by far the most employed method to synthesize Fe_3O_4 nanoparticles [1,9]. Precipitation–oxidation of ferrous hydroxide, first reported by Sugimoto and Majitevic in 1980 [10], is also a widely applied aqueous-based synthesis route [11–15]. The differences between the iron sources in both procedures trigger distinct mechanisms for the Fe_3O_4 nanoparticles formation, yielding products of different sizes. Typically, co-precipitation produces nanoparticles between 5 nm and 15 nm [9,16] while precipitation–oxidation can generate products as large as 1000 nm [11]. For the latter method, the manipulation of the synthesis conditions, like the ratio between the concentrations of the oxidant and the iron precursor, defines the nanoparticle size [11,14,15]. Despite this widespread use and the long-range of diameters achievable during the synthesis, both methods do not provide good control over crystallinity and size distribution of the nanoparticles in comparison with the most recently reported methods. In this sense, the search of alternatives and modifications that can improve these classical aqueous-based procedures has become a challenge of particular interest, especially after the technological applications revealed in the last years.

In order to develop a successful synthetic procedure, two main goalshave to be achieved: first, the size and shape distribution must be as predictable and narrow as possible, and second, aggregation of the nanoparticles must be avoided. The incorporation of stabilizing agents during nanoparticles formation can help to accomplish both objectives. Diverse materials have been studied as stabilizing agents for IONPs. Taking advantage from its various carboxylic groups, citric acid has been employed in both co-precipitation [17] and oxidation precipitation [18] methods, with good results. Employing the latter synthetic method, Jing et al. [18] reported that citric acid not only avoids nanoparticle aggregation, but different concentrations of this compound can also control and define the nanoparticle size. Core–shell structures with gold or SiO_2, and polymers like polyethylene glycol, polyethylene imine or chitosan have also been tested in order to procure useful products for technological applications [1].

In this sense, natural starch appears as a very promising material for the controlled synthesis of IONPs. The size and presence of multiple functional groups may provide the adequate interaction strength with IONPs and at the same time prevent further changes of the nanoparticle, exerting an electrosteric function as protection agent [19]. Beside, starch results an attractive material due to its commercial availability at a low cost, and for being environmentally friendly [20,21].

At the moment, starch-coated IONPs obtained by the co-precipitation method have been developed for As(V) removal in environmental remediation [22,23], for controlled release of cisplatin [24] or as magnetic resonance contrast agents in biomedicine [25].

In this study, we investigate the influence of starch in the synthetic process of Fe_3O_4 nanoparticles by the oxidation–precipitation of ferrous hydroxide method. The addition of starch as a kinetically control agent can affect both the size and size distribution of the Fe_3O_4 nanoparticles, and the aggregation state of the obtained products. Also, we compared the performance of other two polymers as control agents in order to relate the chemical properties of the stabilization agent with the final products of the Fe_3O_4 nanoparticles synthesis.

2. Materials and methods

2.1. Iron oxide nanoparticles (IONPs) syntheses

All the reagents used in this work were analytical grade without further purification. Iron (II) sulphate heptahydrate ($FeSO_4{\cdot}7H_2O$, ≥99%, Sigma–Aldrich), sodium nitrate ($NaNO_3$, ≥99%, Anedra), sodium hydroxide (NaOH, 99%, Anedra), soluble starch (reagent grade, Mallinckrodt), polyethylene glycol 6000 (PEG, 99%, Anedra), polyvinyl alcohol (PVA, fully hydrolyzed, Sigma–Aldrich). Deionized water was used in all experiments.

IONPs were prepared by the precipitation–oxidation of ferrous hydroxide method [10], with some modifications. Briefly, 0.278 g of $FeSO_4{\cdot}7H_2O$ were dissolved in 40 mL of water at 80 °C. Under vigorous stirring, 0.01 mol of NaOH and 1×10^{-3} mol of $NaNO_3$ dissolved in 10 mL of water were added dropwise to the Fe(II) solution. The reaction proceeded under stirring conditions at 80 °C for 2 h after the formation of the black dispersion. IONPs from the dispersion were easily separated by a permanent magnet, and then washed with water and air dried. This sample was labeled as SX. For the starch-coating and size control experiments, the same synthetic method was used, except for the addition of a starch solution (1 g in 10 mL of boiling water) at different time periods after the addition of the $NaOH/NaNO_3$ solution. Samples S0, S1, S2, S3 and S4 were prepared corresponded to starch addition time of 0, 30, 90, 150 and 300 s, respectively. The stable dispersions of starch-coated IONPs were magnetically decanted after the addition of acetone, and finally air dried. PEG-coated and PVA-coated samples were prepared with the same procedure.

2.2. Characterization

Absorption spectra were recorded at room temperature on a UV-vis-NIR Shimadzu UV-1603 using a quartz cuvette with 10 mm optical path length. Samples were diluted in water in order to reach Abs values of 0.3–0.5 at 400 nm. Samples for transmission electron microscopy (TEM) images were examined with a JEOL HR-TEM microscope operated at 300 kV (C2Nano, CNPEM, Campinas, Brazil), after dripping 10 μL of nanoparticle dispersion onto the carbon-coated copper grid and air-dried at room temperature. X-ray diffraction (XRD) patterns were obtained by standard Rigaku diffractometer with CuKα radiation. FTIR spectra were obtained at room temperature in the range 400–4000 cm^{-1} employing a Shimadzu infrared spectrometer model IR-Prestige21, averaging 10 scans at a nominal resolution of 4 cm^{-1} and Happ–Genzel apodization using KBr method. Magnetic properties were measured with a superconducting quantum interference device (SQUID, Quantum Design) in a temperature range from 5 to 300 K. A magnetic field of 20 Oe was applied during the zero field cooled (ZFC) and field cooled (FC) measurements. Dynamic light scattering (DLS) measurements were performed in a Brookhaven model Z Plus equipment, in aqueous dispersions at 25 °C for 10 min ($n = 5$). Correlation functions were analyzed with the Particle Solutions v.2.5 software. Remaining Iron oxide mass was determined by Thermogravimetric Analyzer TGA-50 under static air atmosphere at a heating rate of 10 °C/min.

3. Results and discussion

3.1. Starch-coated IONPs

As an alternative to the Fe(II)/Fe(III) co-precipitation method, the synthesis of magnetite nanoparticles by ferrous hydroxide precipitation–oxidation have some features that make it more suitable to accomplish certain objectives. For instance, particle sizes in

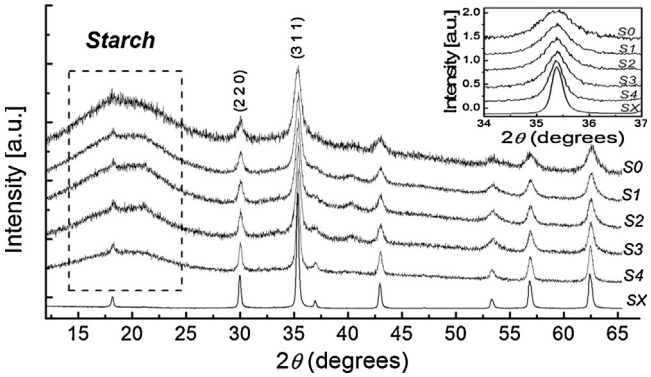

Fig. 1. X-ray diffraction patterns of SX and starch-coated Fe_3O_4 nanoparticles. The crystal grain sizes calculated from Scherrer's equation for the strongest diffraction peak ([3 1 1] at 35.4 degrees, highlighted in the superior inset) are 12 nm for S0, 15 nm for S1, 18 nm for S2, 25 nm for S3, 30 nm for S4, and 40 nm for SX.

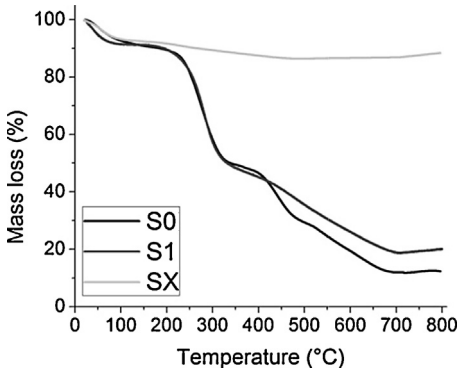

Fig. 2. TGA measurements of samples S0, S1 and SX.

the range between 12 and 100 nm can be easily controlled simply by the addition of starch as a capping agent during the first steps of the reaction. In the well-documented SX sample synthesis procedure (without stabilization agents) [10,14], the excess of OH^- ions maintains the pH well above the isoelectric point of Fe_3O_4 (6.5–6.8) and the charge of the growing particles prevents their aggregation. In this case, particles slowly grow from few seed precursors by the addition of the species in solution, yielding bigger particles compared to the Fe(II)/Fe(III) co-precipitation. This relatively slow nanoparticle aging can be advantageously used to kinetically control the nanoparticle size by the addition of a stabilization agent at different times, in order to freeze the nanoparticle growth and thus control nanoparticle size. This kind of kinetic control was successfully tested in several nanoparticle syntheses, both for size and shape control [26]. In this sense, the addition of a hydrophilic polymer that would provide a significant steric hindrance (like starch) can affect both the seed nucleation and aging process, preventing the formation of larger nanoparticles and stabilizing intermediate-sized products.

A series of samples were prepared in order to investigate the role of starch as a controlling agent of the growth kinetics of the Fe_3O_4 nanoparticle seeds. The crystalline structures of the samples were characterized by X-ray diffraction (Fig. 1). The uncoated sample (SX) diffractogram matches well with the Fe_3O_4 crystalline pattern and confirms the formation of the *fcc* spinel-inverse iron oxide phase. The narrow Bragg peaks indicates a large order of diffracting planes, which is related to bigger crystallite grain and nanoparticles size. For this sample, crystal size is about 40 nm. Starch-coated samples (S0, S1, S2, S3 and S4) show two contributions on the XRD patterns. First, broad diffraction peaks associated to Fe_3O_4 crystalline structure phase can be seen in all samples, confirming the formation of Fe_3O_4 nanostructures. Also, as we can see more precisely in the inset of Fig. 1 (diffraction peak corresponding to (3 1 1) plane), there is clear inverse correlation between the increasing addition time of the starch solution and the Fe_3O_4 peaks width. We used the Scherrer equation to estimate the mean crystal grain size of the samples employing this strongest diffraction peak. In starch-coated samples, the grain size increased dramatically, from 12 nm for sample S0 to 30 nm for sample S4, as we delay the addition of the stabilization agent. Second, a very broad peak with a maximum at 15° is related to the presence of starch molecules, coating the Fe_3O_4 nanoparticles. The drying and magnetically assisted washing procedure ensures no free-starch was left in the in the final solid sample; hence the starch evidenced in the XRD pattern must be somehow attached to the Fe_3O_4 nanoparticles. As Fig. 1 shows, the relative intensity and total area assigned to both Fe_3O_4 and starch contributions vary in each sample. For the normalized patterns, the starch contribution decreases as the particles get bigger. This difference can be explained by assuming that total starch in the sample is related to IONPs surface and not to IONPs mass. For the same amount of Fe_3O_4, smaller nanoparticles have a higher surface total area, thus allowing the attachment of a bigger number of starch molecules to the nanoparticle system. TGA measures of samples S0, S1 and SX (Fig. 2) supplement this idea since total mass loss (related to total amount of organic coating) is bigger for the smaller particles (90% of mass loss for S0 and 80% of mass loss for S1). Also, IR spectroscopy (Fig. 3) confirms the attachment of starch on the Fe_3O_4 surface. In summary, the peaks width and the starch proportion from the XRD patterns, and the TGA results confirm the coating and size-control by starch of the Fe_3O_4 nanoparticles.

In addition, electron microscopy images (SEM and TEM) of samples SX and S0 (Fig. 4) reveal the different sizes of the final products obtained in each synthesis. For the uncoated Fe_3O_4 sample (SX), particles of bigger size are obtained. SEM images show a particle population with a mean diameter of approximately 100 nm, with a relatively wide size distribution. The difference between this value and the one obtained from Scherrer equation may be caused by the polycrystallinity of the Fe_3O_4 particles. Because these particles are composed by various crystal grains, the latter size (obtained by Scherrer equation from XRD patterns) is lower than the total size of the nanoparticle obtained by SEM images. TEM images of sample S0 show well-dispersed particles of smaller size (ca. 15 nm diameter) and narrower size distribution. This result is in good agreement with the size calculated via Scherrer equation. Also, the absence of agglomerated structures in the images confirms the stabilization role of starch, as it helps to avoid the formation of nanoparticle clusters, even in the solid state. Hydrodynamic size of starch coated IONPs were measured by DLS, and the results follows the same tendencies detailed above. S0 effective mean diameter is 93 ± 2 nm

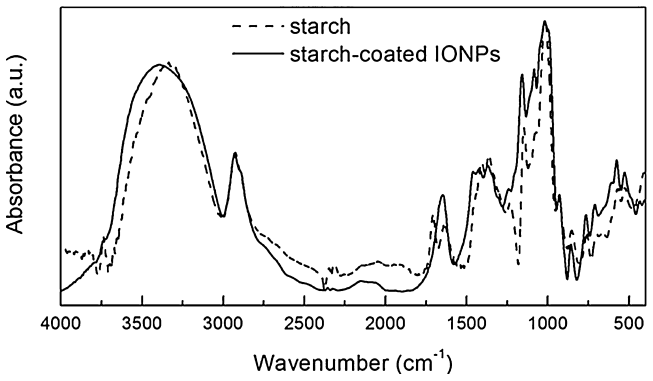

Fig. 3. FTIR spectra of pure starch and starch-coated Fe_3O_4 nanoparticles (sample S1).

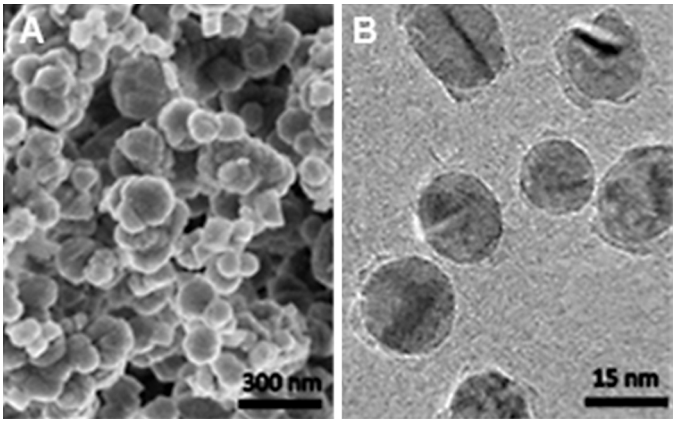

Fig. 4. (A) SEM image of Fe_3O_4 nanoparticles from SX sample. (B) TEM image of starch-coated Fe_3O_4 nanoparticles from S0 sample.

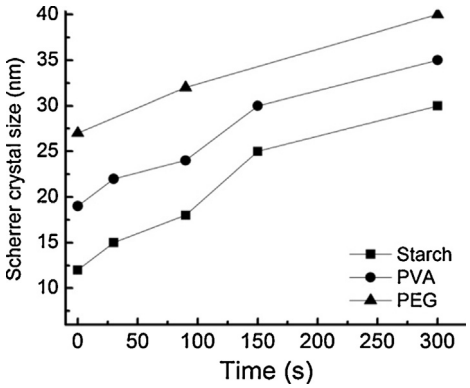

Fig. 6. Plot of the Scherrer crystal size of the Fe_3O_4 nanoparticles obtained in the synthesis versus the addition time of the corresponding polymer in the mixture reaction.

with a standard deviation of 1.15 nm ($n = 5$). This size is way larger than IONPs diameter deduced by TEM images and evidences the massive starch coating over the nanoparticle. Similar mean diameter was reported by Soshnikova et al. [27] for starch-coated IONPs prepared by co-precipitation, with starch added before nanoparticle formation. As particles get bigger so does the hydrodynamic size. For S1, mean diameter is 152 ± 5 nm and for S2 is 334 ± 12 nm ($n = 5$). Samples S3 and S4 were above 400 nm. For all samples, mean effective diameter did not change within a week between measures. The addition of starch after IONPs formation was also studied by Soshnikova et al. [27], with similar results. Despite the difference between the employed IONPs synthesis method, the addition of the polymer after the reaction beginning always yields bigger hydrodynamic size. In our case, this trend can be consequence of starch addition time as reported by Soshnikova et al. but also it is consequence of bigger IONPs size.

The stability of the colloidal samples was assessed by UV–vis spectroscopy. As Fig. 5 shows, the absorption at 400 nm of water-redispersed powders from S0 sample hardly changes during a week of measures, attesting the colloidal stability over-time of the synthesis products. The UV–vis spectrum of S0 is also shown in Fig. 4. Same behavior is observed for starch-coated samples S1 and S2, but for S3 and S4 absortion start to decline after the third day. Both van der Waals forces and electrostatic attractions are the main cause of the colloidal system stability, as they dominate the interaction between starch and Fe_3O_4 nanoparticles surface. As a typical dipole–dipole relation, the electron-rich hydroxyl groups of starch molecules strongly interact with the electron-deficient Fe atoms in the oxide surface, generating the organic-coating over the nanoparticle. Also, starch hydrophilic hydroxyl groups ensure the stabilization and water dispersion of coated-Fe_3O_4.

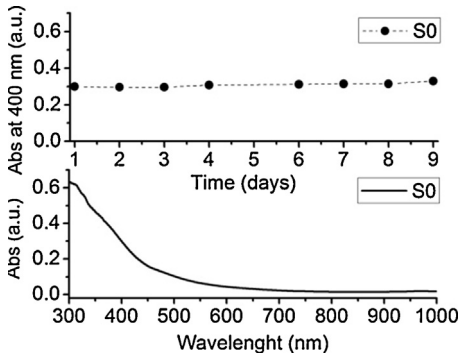

Fig. 5. Absorbance at 400 nm versus standing time (upper panel) and UV–vis absorption spectra (lower panel) of an aqueous dispersion of starch-coated Fe_3O_4 nanoparticles from sample S0.

3.2. PEG & PVA vs. starch as polymer-assisted size control agents

The polymer chemical nature plays an important role on the size and aggregation control of the nanoparticles. To study this influence, similar experiments were carried out with polyethylene glycol (PEG) and polyvinyl alcohol (PVA) instead of starch.

For the samples series with PEG, the size control effect over the Fe_3O_4 nanoparticles was less effective in comparison with the previous starch discussed samples. In XRD patterns of these products, the narrowing of the Fe_3O_4 Bragg peaks was less pronounced that in the starch series, showing a decline in the impact of the polymer-addition time in the final nanoparticle size. The Scherrer-calculated nanocrystal grain size increases from 27 nm for $S0_{PEG}$ to 40 nm for $S3_{PEG}$ in the PEG-coated series (Fig. 6). As we can see, the smaller PEG-sample grain size, $S0_{PEG}$, almost doubles the one obtained with starch for the same polymer-addition time. Also, the last sample has a similar grain size than the uncoated Fe_3O_4 preparation. Unlike the starch samples, the absence of strong electronegative groups in PEG molecules inhibits the intense dipolar interaction between the iron oxide surface and the polymer needed to stop the growth of the nanoparticle. As a result, the evolution of small crystal seeds to bigger particles is favored over the stabilization of intermediate-size elements by the added polymer.

To complement previous results, PVA was also used as a growth controller. PVA-coated Fe_3O_4 nanoparticles series have a similar size-control behavior than the starch-coated samples (Fig. 6); however, for the same polymer-addition time, all the Fe_3O_4 crystal sizes in the PVA samples are bigger (typically 5–7 nm) than the corresponding starch sample. Like starch molecules, the high density of hydroxyl groups among the PVA polymer can produce the interactions required to stop the growth of the Fe_3O_4 nanoparticles by a similar chemical mechanism. The differences in size between these two series, however, can be attributed to a bigger steric contribution from the polymer in starch samples compared to PVA samples. The monomer dimensions (glucose in starch against vinyl alcohol in PVA) and the number of hydroxyl groups per monomer (five in glucose against one in vinyl alcohol) reveal these contrasts in the steric contributions and generate the differences between the Fe_3O_4 crystal grain sizes in both series.

Also, it is important to highlight that the starch-coated samples were the only ones that can be easily dispersed in water, producing a water-based ferrofluid stable for several weeks. Unlike typical reports on PVA and PEG-coated IONPs, our nanoparticles are hardly water dispersible for long time ranges, and only stand within

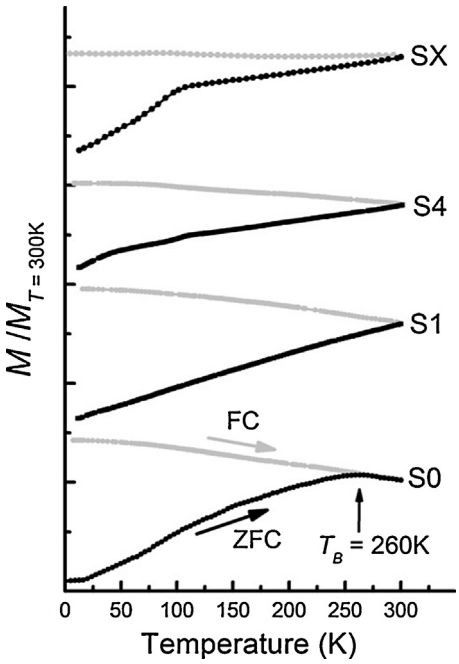

Fig. 7. Zero field cooled (ZFC) and field cooled (FC) curves for starch-coated and uncoated Fe_3O_4 nanoparticles. All curves are normalized to magnetization at $T = 300$ K.

the solvent for a couple of days. For co-precipitation synthetized IONPs colloidal stabilization by a polymer is a well-known behavior [28,29], but for oxidation–precipitation products these characteristic is less studied. For these cases, formation of bigger and probably polycrystalline IONPs beats the stabilization by the coating agent, leading to the precipitation of the nanoparticles. Nevertheless, PVA and PEG-coated IONPs were several orders more stable than non-coated oxidation–precipitation IONPs (two days for coated samples against seconds for uncoated ones)

3.3. Magnetic characterization

Fig. 7 shows the ZFC/FC curves measured at 20 Oe from 5 K to 300 K. As the particle size and aggregation state of the system has great influence on the magnetic properties, the ZFC/FC curves of the starch-coated and uncoated samples were expected to exhibit different magnetic behaviors. Also, because measures were made in dried-solid samples, dipolar interactions may be expected due to the spatial approach and agglomeration produced by the elimination of the matrix solvent [30–32]. S0, S1 and S4 curves can be considered as diverse cases of interacting magnetic nanoparticle systems, while SX is a typical curve of a highly interacting percolated magnetic system [33,34]. For the latter, two approximately linear growths with a slope-change at ca. 107 K are observed in the ZFC magnetization curve. This behavior could be linked to the presence of two populations of aggregates of different size in the sample.

The zero-field magnetization curve for S0 displays a broad maximum at $T = 260$ K. This temperature is related to the so-called blocking temperature (T_B) and shows the transition between the blocked and the superparamagnetic state. When $T > T_B$, the thermal energy exceeds the anisotropy energy, leading to a randomization of the magnetic moments much faster than the experimental time scales [35]. The measured T_B is in good agreement with literature reports on weakly interacting systems based in Fe_3O_4 nanoparticles of approximately 15 nm [36,37].

The contrast in the magnetic behavior of samples SX and S0 is also supported by M vs. H measure (Fig. 8). The coercive field

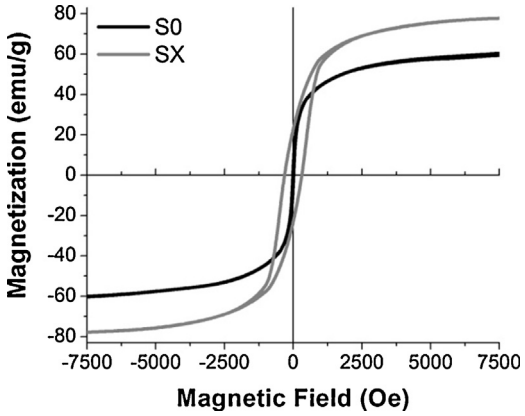

Fig. 8. M vs. H curve at $T = 273$ K of S0 and SX.

in SX confirms the blocked regime of this sample at 273 K, while the absence of hysteresis loop in S0 indicates a superparamagnetic behavior. The observed difference between saturation magnetization (expressed as IONPs mass) is also consequence of nanoparticle size. Saturation for SX is near the value for bulk magnetite due to massive nanoparticle volume. In the other hand, the reduction of saturation for S0 is consequence of significant contribution of the magnetic moments disorder within the IONPs surface [38]. Real saturation for powder sample S0 is 11.7 emu/g.

Assuming S0 is a non-aggregated nanoparticles system (by TEM images evidence), a weakly interacting magnetic behavior can be proposed and a quantitative approach value of the effective anisotropy constant can be obtained using the Bean–Livingston equation [39]:

$$T_B = \frac{K_{eff} V}{25 k_B} \quad (1)$$

where k_B is the Boltzmann constant and V is the particle volume. The calculated number ($K_{eff} = 5.07 \times 10^4\ J\,m^{-3}$) is close to values reported in the literature for weakly interacting Fe_3O_4 nanoparticles [40]. In samples S1 and S4 the absence of a maximum in the ZFC curve indicates that the blocking temperature is above 300 K, due to bigger particle size and/or possible aggregation. This magnetic behavior in ZFC-FC curves with an applied field of 20 Oe is expected for Fe_3O_4 with a nanoparticle diameter above ca. 18 nm [30,38]. In these samples, the nanoparticles are not on the superparamagnetic regime at room temperature; the observed blocked behavior is consequence of the bigger Fe_3O_4 magnetic nanoparticles and the dipolar interactions among them. Between these two samples, the ZFC curve of S1 has a more monotonous growth compared to the irregular increase in the S4 ZFC magnetization. This observation can be explained by assuming the starch size-dispersion and agglomeration control is more effective when the reagent is introduced at the beginning of reaction, thereby reducing the formation of clusters of smaller seeds and polycrystalline nanoparticles. The relation between the TEM/SEM images size and the Scherrer grain size in samples S0 and SX discussed before also supports these observations. The proposed better size-dispersion and agglomeration control at early stages is also helpful to explain the magnetic behavior of S0.

4. Conclusions

A chemical control process mediated by a polymer was proposed to define the size and aggregation of Fe_3O_4 nanoparticles synthetized by the precipitation–oxidation of ferrous hydroxide method. The addition of starch at different times after the beginning of the synthesis can stop the nanoparticle growth, and yield

starch-coated Fe_3O_4 nanoparticles of different size. Also, starch hydrophilic-coating assures good water-dispersion stability and possible biocompatibility.

The kinetic control assays with PEG and PVA shows that the polymer nature, defined by the electrosteric hindrance and the monomer chemical groups, plays an important role on the size and aggregation of the nanoparticles. This kinetic effect is more pronounced for voluminous polymers with many charged groups per monomer, like starch.

Acknowledgments

We acknowledge the financial support from National Research Council (CONICET) and National Agency for the Promotion of Science and Technology (ANPCyT) from Argentina, and the support from PEDECIBA (PNUD/URU/97016), CSIC and ANII from Uruguay. Laboratorio de Biomateriales belongs to the Centro Interdisciplinario en Nanotecnología, Química, y Física de Materiales, Espacios Interdisciplinarios, UdelaR. We would like also to thank D. Muraca (LMBT, Campinas, Brazil) & M. M. Gómez-Hermida (UNAL, Colombia) for TEM images and María José Batiller for TGA measurements. O. Moscoso-Londoño also thanks to COLCIENCIAS, Colombia.

References

[1] S. Laurent, D. Forge, M. Port, A. Roch, C. Robic, L.V. Elst, R.N. Muller, Magnetic iron oxide nanoparticles: synthesis, stabilization, vectorization, physicochemical characterizations, and biological applications, Chem. Rev. 108 (2008) 2064.
[2] I. Koh, L. Josephson, Magnetic nanoparticle sensors, Sensors 9 (2009) 8130.
[3] Q.A. Pankhurst, J. Connolly, S.K. Jones, J. Dobson, Applications of magnetic nanoparticles in biomedicine, J. Phys. D: Appl. Phys. 36 (2003) R167.
[4] O. Veiseh, J.W. Gunn, M. Zhang, Design and fabrication of magnetic nanoparticles for targeted drug delivery and imaging, Adv. Drug Deliv. Rev. 62 (2010) 284.
[5] S. Sun, H. Zeng, Size-controlled synthesis of magnetite nanoparticle, J. Am. Chem. Soc. 124 (2002) 8204.
[6] J. Ge, Y. Hu, M. Biasini, W. Beyermann, Y. Yin, Superparamagnetic magnetite colloidal nanocrystal clusters, Angew. Chem. Int. Ed. 46 (2007) 4342.
[7] W. Cai, J. Wan, Facile synthesis of superparamagnetic magnetite nanoparticles in liquid polyols, J. Colloid Interface Sci. 305 (2007) 366.
[8] N. Moumena, P. Veilletb, M.P. Pileni, Controlled preparation of nanosize cobalt ferrite magnetic particles, J. Magn. Magn. Mater. 149 (1995) 67.
[9] R. Massart, Preparation of aqueous magnetic liquids in alkaline and acidic media, IEEE Trans. Magn. 17 (1981) 1247.
[10] T. Sugimoto, E. Matijević, Formation of uniform spherical magnetite particles by crystallization from ferrous hydroxide gels, J. Colloid Interface Sci. 74 (1980) 227.
[11] Y. Zhang, Z. Ren, Y. Fua, X. Yuan, Y. Zhai, H. Huang, H. Zhai, An investigation on the behavior of fine-grained magnetite particles as a function of size and surface modification, J. Phys. Chem. Solids 70 (2009) 505.
[12] L.Y. Zhang, H.C. Gu, X.M. Wang, Magnetite ferrofluid with high specific absorption rate for application in hyperthermia, J. Magn. Magn. Mater. 311 (2007) 228.
[13] F. Vereda, J.d. Vicente, M.d.P. Morales, F. Rull, R. Hidalgo-Álvarez, Synthesis and characterization of single-domain monocrystalline magnetite particles by oxidative aging of $Fe(OH)_2$, J. Phys. Chem. C 112 (2008) 5843.
[14] F. Vereda, J.d. Vicente, R. Hidalgo-Alvarez, Oxidation of ferrous hydroxides with nitrate: a versatile method for the preparation of magnetic colloidal particles, J. Colloid Interface Sci. 392 (2013) 50.
[15] K. Mandel, C. Kolb, M. Straßer, S. Dembskia, G. Sextl, Size controlled iron oxide nano octahedra obtained via sonochemistry and natural ageing, Colloids Surf. A 457 (2014) 27–32.
[16] M. Ma, Y. Wu, J. Zhou, Y. Sun, N.G. Yu Zhang, Size dependence of specific power absorption of Fe_3O_4 particles in AC magnetic field, J. Magn. Magn. Mater. 268 (2004) 33.
[17] S. Campelj, D. Makovec, M. Drofenik, Preparation and properties of water-based magnetic fluids, J. Phys.: Condens. Matter 20 (2008) 204101.
[18] J. Jing, Y. Zhang, J. Liang, Q. Zhang, E. Bryant, C. Avendano, V.L. Colvin, Y. Wang, W. Li, W.W. Yu, One-step reverse precipitation synthesis of water-dispersible superparamagnetic magnetite nanoparticles, J. Nanopart. Res. 14 (2012) 827.
[19] S. Botasini, E. Méndez, Silver nanoparticle aggregation not triggered by an ionic strength mechanism, J. Nanopart. Res. 15 (2013) 1526.
[20] D.K. Kim, M. Mikhaylova, Y. Zhang, M. Muhammed, Protective coating of superparamagnetic iron oxide nanoparticles, Chem. Mater. 15 (2003) 1617.
[21] T.T. Dung, T.M. Danh, L.T.M. Hoa, D.M. Chien, N.H. Duc, Structural and magnetic properties of starch-coated magnetite nanoparticles, J. Exp. Nanosci. 4 (2009) 259.
[22] B. An, Q. Liang, D. Zhao, Removal of arsenic(V) from spent ion exchange brine using a new class of starch-bridged magnetite nanoparticles, Water Res. 45 (2011) 1961.
[23] M. Zhang, G. Pan, D. Zhao, G. He, XAFS study of starch-stabilized magnetite nanoparticles and surface speciation of arsenate, Environ. Pollut. 159 (2011) 3509.
[24] S. Likhitkar, A.K. Bajpai, Magnetically controlled release of cisplatin from superparamagnetic starch nanoparticles, Carbohydr. Polym. 87 (2012) 300.
[25] M.R. Saboktakin, A. Maharramov, M.A. Ramazanov, Synthesis and characterization of superparamagnetic nanoparticles coated with carboxymethyl starch (CMS) for magnetic resonance imaging technique, Carbohydr. Polym. 78 (2009) 292.
[26] S. Botasini, E.A. Dalchiele, J.C. Benech, E. Méndez, Stabilization of triangular and heart-shaped plane silver nanoparticles using 2-thiobarbituric acid, J. Nanopart. Res. 13 (2011) 2819.
[27] Y.M. Soshnikova, S.G. Roman, N.A. Chebotareva, O.I. Baum, M.V. Obrezkova, R.B. Gillis, S.E. Harding, E.N. Sobol, V.V. Lunin, Starch-modified magnetite nanoparticles for impregnation into cartilage, J. Nanopart. Res. 15 (2013) 2092.
[28] K. Mandel, F. Hutter, C. Gellermann, G. Sextl, Synthesis and stabilisation of superparamagnetic iron oxide nanoparticle dispersions, Colloids Surf. A 390 (2011) 173–178.
[29] S. García-Jimeno, J. Estelrich, Ferrofluid based on polyethylene glycol-coated iron oxide nanoparticles: characterization and properties, Colloids Surf. A 420 (2013) 74–81.
[30] M. Knobel, W.C. Nunes, L.M. Socolovsky, E.D. Biasi, J.M. Vargas, J.C. Denardin, Superparamagnetism and other magnetic features in granular materials: a review on ideal and real systems, J. Nanosci. Nanotechnol. 8 (2008) 2836.
[31] J.M. Vargas, L.M. Socolovsky, M. Knobel, D. Zanchet, Dipolar interaction and size effects in powder samples of colloidal iron oxide nanoparticles, Nanotechnology 16 (2005) S285–S290.
[32] O. Moscoso-Londoño, M.S. Carrião, C. Cosio-Castañeda, V. Bilovol, L.M. Socolovsky, R.M. Sánchez, E.J. Lede, R. Martínez-García, One-step room temperature synthesis of very small γ-Fe_2O_3 nanoparticles, Mater. Res. Bull. 48 (2013) 3474.
[33] S. Bedanta, W. Kleemann, Superparamagnetism, J. Phys. D: Appl. Phys. 42 (2009) 013001.
[34] L.M. Socolovsky, F.H. Sánchez, P.H. Shingu, Magnetic structure of FexCu100–x magnetoresistive alloys produced by mechanical alloying, Hyperfine Interact. 133 (2001) 47–52.
[35] C. Schweiger, C. Pietzonka, J. Heverhagen, T. Kissel, Novel magnetic iron oxide nanoparticles coated with poly(ethyleneimine)-g-poly(ethylene glycol) for potential biomedical application: synthesis, stability, cytotoxicity and MR imaging, Int. J. Pharm. 408 (2011) 130.
[36] A.M. AL-Baradi, O.O. Mykhaylyk, H.J. Blythe, M. Geoghegan, Magnetic field dependence of the diffusion of single dextran molecules within a hydrogel containing magnetite nanoparticles, J. Chem. Phys. 134 (2011) 094901.
[37] D. Caruntu, G. Caruntu, C.J. O'Connor, Magnetic properties of variable-sized Fe_3O_4 nanoparticles synthesized from non-aqueous homogeneous solutions of polyols, J. Phys. D: Appl. Phys. 40 (2007) 5801.
[38] J.M.D Coey, Noncollinear spin arrangement in ultrafine ferrimagnetic crystallites, Phys. Rev. Lett. 27 (1971) 1140.
[39] C.P. Bean, J.D. Livingston, Superparamagnetism, J. Appl. Phys. 30 (1959) 120.
[40] D. Fiorani, A.M. Testa, F. Lucari, F. D'Orazi, H. Romero, Magnetic properties of maghemite nanoparticle systems: surface anisotropy and interparticle interaction effects, Phys. B 320 (2002) 122.